Estimation of Ice Hydrometeor Types and Shapes from Radar Polarization Measurements

SERGEY Y. MATROSOV

Cooperative Institute for Research in the Environmental Sciences, University of Colorado and NOAA/ETL, Boulder, Colorado

ROGER F. REINKING, ROBERT A. KROPFLI, AND BRUCE W. BARTRAM

NOAA Environmental Technology Laboratory, Boulder, Colorado

(Manuscript received 29 December 1994, in final form 15 June 1995)

ABSTRACT

An approach to distinguish between various types of ice hydrometeors and to estimate their shapes using radar polarization measurements is discussed. It is shown that elevation angle dependencies of radar depolarization ratios can be used to distinguish between planar crystals, columnar crystals, and aggregates in reasonably homogeneous stratiform clouds. Absolute values of these ratios depend on the reflectivity-weighted mean particle aspect ratio in the polarization plane. Circular depolarization ratios depend on this ratio, and linear depolarization ratios depend on this ratio and particle orientation in the polarization plane. The use of nearly circular elliptical polarization provides a means of measuring depolarization for low reflectivity scatterers when the circular polarization fails due to low signal level in one of the receiving channels. Modeling of radar backscattering was applied to the elliptical depolarization ratios as measured by the K_a-band radar developed at the NOAA Environmental Technology Laboratory. Experimental data taken during the Winter Icing and Storms Instrument Test experiment in 1993 generally confirmed the calculations and demonstrated the applicability of the approach.

1. Introduction

Ice clouds and precipitation consist of hydrometeors of different types, shapes, sizes, and bulk densities. The particle types in ice clouds and in solid precipitation vary from single pristine crystals to complex aggregates. Particles of the same type can have different ratios of dimensions along their principal axes. The wide range of values that these parameters can take makes it particularly difficult to determine remotely cloud microphysical properties. A rather comprehensive ice hydrometeor classification scheme was first introduced by Magono and Lee (1966). Their classification diagram has been repeatedly published by different authors (for example, see Pruppacher and Klett 1978) and is used throughout this work.

Knowledge of ice particle sizes, types, and their characteristic aspect ratio (shape) is important in studies of climate, aircraft icing, and water resources. These parameters influence optical characteristics such as single-scattering albedo and asymmetry factor, which in turn determine the shortwave radiative transfer (Liou and Takano 1994). Shape parameters are also important for estimating infrared optical properties of ice clouds (Chylek and Videen 1994), which govern the longwave radiative transfer.

Corresponding author address: Dr. Sergey Y. Matrosov, 325 Broadway, R/E/ET6, Boulder, CO 80303.

Some recent studies (Dungey and Bohren 1993; Fu and Liou 1993; Schneider and Stephens 1994) show that the details of particle shape may not be critical in scattering and absorption calculations. It appears, however, that the general shape (i.e., particle aspect ratio) and type (e.g., planar or columnar type crystals) are important in estimating particle optical and radiative properties. Accounting for nonsphericity is especially important for scattering calculations in different wavelength regions.

The formation and maintenance of supercooled liquid water in clouds is compensated by nucleation and growth of ice crystals. Ice crystal initiation and growth rate along with particle shape, type, and the consequent consumption rates of the liquid are all dependent on temperature and supersaturation. Thus, in monitoring and forecasting icing conditions hazardous to aircraft, for example, knowledge of both the presence and type of ice crystals is important. Furthermore, for the same reasons, the shape of particles in solid precipitation is important for understanding evolution and water budget of winter storms. As suggested by Mason (1994), transitions between different types of ice crystals (e.g., plates, dendrites, columns) occurring in clouds can permit more effective release of precipitation through formation of precipitation elements that have a better chance of surviving evaporation below cloud base.

Until recently, the only way to obtain information on ice particle types and their shapes was by sampling

particles in situ with ground-based or airborne instruments. In recent years, however, progress has been made in developing remote sensing methods for estimating particle shapes and types. Methods based on the polarization state of radar echoes have good potential for distinguishing and identifying different ice hydrometeor species. Several such algorithms for particle identification (rain, hail, graupel, snow, high-density crystals) in severe convective storms are given in Doviak and Zrnić (1993). These algorithms are based on analysis of several linear polarization parameters such as differential reflectivity, copolar correlation coefficient, differential phase shift, and linear depolarization ratio observed with a 10-cm-wavelength radar.

Millimeter-wavelength radars have an advantage over conventional centimeter-wavelength radars in sensing low reflectivity, nonprecipitating ice clouds, and light and moderate snowfalls. Even though some longer-wavelength radars, such as the WSR-88D, have nearly the same sensitivity to clouds as millimeter-wavelength radars, the latter provide much better spatial resolution and significantly less clutter (Kropfli and Kelly 1995) allowing them to be used at very close ranges.

The National Oceanic and Atmospheric Administration's Environmental Technology Laboratory (NOAA ETL) K_a-band ($\lambda \approx 8.6$ mm) cloud-sensing radar (Kropfli et al. 1990), which is used here to demonstrate the approach developed below, is able to detect a −30-dBZ echo at 10 km, fine spatial resolution (37.5-m pulse width and 0.5° beamwidth). These attributes, in addition to its polarization agility, make this radar an excellent tool for cloud and light or moderate ice precipitation studies. Polarization agility of this radar is achieved by rotation of a phase-retarding plate (PRP). If the plate phase shift is exactly 90°, that is, a quarter wave plate, possible polarization states of transmitted signals are horizontal (achieved with the horizontal or vertical orientations of the PRP), left-hand and right-hand circular (achieved when the PRP is oriented at 45°, 135°, 225°, or 315°), and different states of elliptical polarization. For these elliptical polarizations, the ellipticity angle is equal to the orientation angle of the polarization ellipse (Matrosov and Kropfli 1993).

Two remote sensing approaches to estimate ice particle shapes from radar measurements with elliptical polarizations were suggested in Matrosov and Kropfli (1993) and Matrosov (1991b). Initial experimental evidence provided in Reinking et al. (1995) shows that hydrometeor types can indeed be identified by using the polarization agile K_a-band radar measurements and matching them to the earlier theoretical results (Matrosov 1991a). In the work presented here, we extend some of these theoretical considerations and illustrate applicability of new approaches for differentiating ice hydrometeor types and estimating their shapes with radar data taken near Platteville, Colorado, during the Winter Icing and Storms Project Instrument Test (WISPIT) in 1993.

2. Radar measurables and phase-retarding plate calibrations

a. Backscattering polarization parameters

The amplitude (Jones) polarization matrix $\mathbf{R}$ of the ETL K_a-band radar PRP in the linear horizontal–vertical (HV) basis is (Matrosov and Kropfli 1993)

$$\mathbf{R}(\beta, \Psi) = \begin{vmatrix} \cos\beta & -\sin\beta \\ \sin\beta & \cos\beta \end{vmatrix} \begin{Vmatrix} \exp(i\Psi) & 0 \\ 0 & 1 \end{Vmatrix} \begin{vmatrix} \cos\beta & \sin\beta \\ -\sin\beta & \cos\beta \end{vmatrix}, \quad (1)$$

where β and Ψ are the PRP rotation and phase-shift angles, respectively. The first and third matrices in (1) rotate the reference HV basis to the linear basis along the PRP principal axes and back. The second matrix in (1) describes the phase shift introduced by the PRP. If the polarization incident on the PRP is horizontal, the amplitude vector $\mathbf{P}$ of transmitted radar signals will be the following:

$$\mathbf{P} = \begin{vmatrix} e^{i\Psi}\cos^2\beta + \sin^2\beta \\ e^{i\Psi}\sin\beta\cos\beta - \sin\beta\cos\beta \end{vmatrix}. \quad (2)$$

The combined effects of hydrometeor scattering and the transformations by the PRP on the transmitted and received signals are given by the matrix $\mathbf{Y}$:

$$\mathbf{Y} = \mathbf{R}(-\beta, \Psi)\mathbf{S}\mathbf{R}(\beta, \Psi), \quad (3)$$

where $\mathbf{S}$ is the hydrometeor amplitude scattering matrix. This matrix as applied to ice hydrometeors is described in detail in Matrosov and Kropfli (1993). Propagation effects in ice clouds and snow can usually be neglected for propagation paths in scattering media of up to several kilometers (Matrosov 1991b). Neglecting propagation effects in such cases can result in errors in estimating depolarization ratios of less than 1 dB that is acceptable for most applications. We accordingly will ignore propagation effects for modeling and data analysis in this work, limiting our observations to relatively close ranges.

The ETL K_a-band radar has a two-channel receiver that allows reception of echoes having the same polarization as the transmitted signals simultaneously with the polarization orthogonal to the transmitted polarization. The depolarization ratio DR is defined as a logarithmic ratio of received power in these two channels and can be expressed by elements of the matrix $\mathbf{Y}$ (Matrosov and Kropfli 1993):

$$\mathrm{DR}(\beta, \Psi) = 10\log_{10}\left(\frac{\langle|y_{11}|^2\rangle}{\langle|y_{12}|^2\rangle}\right), \quad (4)$$

where angle brackets represent averaging with respect to particle sizes, shapes, and orientations. The depo-

larization ratio depends on the hydrometeor properties and on the PRP orientation (β) and phase-shift (Ψ) angles. Note that $\Psi = 90°$ and $\beta = 45°$ provide circular depolarization ratio (CDR), and any Ψ and $\beta = 0°$ (or 90°) provide linear depolarization ratio (LDR).

b. *Calibration of the phase-retarding plate*

To determine the true phase shift of the PRP, a known source of linear polarization with the polarization plane tilted 45° from the vertical was used to illuminate the antenna for two positions of the PRP, $\beta = 0°$ and $\beta = 90°$. This procedure showed that the PRP phase shift was $\Psi = 79° \pm 2°$ rather than the 90° intended by the plate design. A calibration on natural scatterers was also performed to confirm this finding. Ideal natural scatterers for such calibrations are small drizzle drops having nearly spherical shapes. These additional PRP calibration measurements were performed on 6 April 1993, in uniform drizzle during WISPIT in northeastern Colorado.

Figure 1 shows the DR obtained in drizzle as a function of the PRP rotation angle β. Drizzle drops are spherical Rayleigh scatterers for the 8.6-mm-wavelength radar. The PRP was rotated at a rate one revolution in 2 min, and data were taken at 250-m range. As expected for spherical scatterers, the results were similar for all radar elevation angles χ. Due to the inversion of the propagation direction, right-hand circular polarization is scattered as left-hand circular. Thus, the larger of the two circularly polarized received signals is in the channel with the polarization that is orthogonal to the transmitted one, and the ratio DR, as defined in (4), is negative; DR for linear polarization is positive. Thus, the sign of the depolarization ratio is different for measurements of LDR and CDR as defined in (4) and can be seen in Fig. 1.

It can be seen also from Fig. 1 that for horizontal polarization ($\beta = 0°$ or $\beta = 90°$) DR approaches about 35 dB, which is, evidently, the polarization channel isolation of the radar–antenna system. Results of calculations for small spherical water drops are also depicted in Fig. 1. Theoretical results are plotted for the PRP phase shifts of $\Psi = 90°$ and $\Psi = 79.5°$. The same level of polarization isolation, 35 dB, was assumed for all orientation angles β. It can be seen that the theoretical results for $\Psi = 79.5°$ are in a very good agreement with the experimental data that is also very close to the value obtained from the direct antenna illumination test, $79° \pm 2°$. Based on this agreement, the value $\Psi = 79.5°$ was used when interpreting radar polarization data taken with this PRP.

It should be noted, however, that some uncertainty still remains in matching experimental and theoretical data because of errors in depolarization measurements. An uncertainty in such matching can be roughly estimated as about $\pm 0.5°$ in the PRP phase shift Ψ. An assumption that $\Psi = 79.5°$ gives the theoretical value

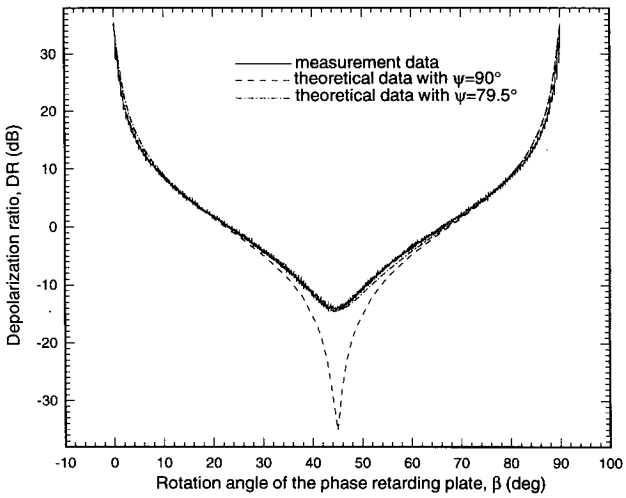

FIG. 1. Drizzle calibration of the NOAA K_a-band radar phase retarding plate.

of DR for small spherical scatterers about −14.8 dB ($\beta = 45°$). Assumptions that $\Psi = 79°$ and $\Psi = 80°$ would yield about −14.3 and −15.2 dB for this value, respectively.

c. *The use of elliptical polarization versus circular and linear*

The use of conventional depolarization measurements (i.e., CDR or LDR) to infer ice hydrometeor types and shapes has been discussed in Matrosov (1991a). For common particle orientations, CDR is usually greater than LDR; that is, the signal-level difference between two receiving channels is generally less for circular polarization than for linear. CDR depends on the reflectivity-weighted mean particle aspect ratio projected on the incident wave polarization plane. LDR depends on this ratio and also on the particle orientation in this plane. This suggests that, for the purpose of estimating the shapes of hydrometeors, circular polarization is preferable to linear polarization.

When, the circular polarization is used, the "weak" echo is usually substantially less (up to several orders of magnitude) than the "strong" one and is often below the radar detectability threshold. This makes the use of the circular polarization for estimating hydrometeor shapes impossible in many situations of interest (e.g., nonprecipitating clouds). It was suggested in Matrosov and Kropfli (1993) that this problem can be avoided with the use of certain elliptical polarization states that are nearly circular. These polarizations have an advantage because of an increase in the intensity of the weak channel that provides better signal-to-noise ratio in this channel while the strong channel signal is nearly unchanged (usually within a few tenths of 1 dB).

The ability of the NOAA K_a-band radar to transmit different polarizations is achieved by rotating the PRP

to a new angle β and/or changing the PRP phase shift Ψ. Note, that Ψ can be changed only by installing a different phase-retarding plate. Elliptical polarizations achievable by changing β from 45° to 43° or to 41° were discussed in Matrosov and Kropfli (1993). The analysis presented here is extended for elliptical polarizations obtainable by changing the PRP phase shift Ψ. The orientation of the polarization ellipse of these elliptical polarizations is horizontal (for $\Psi < 90°$) or vertical (for $\Psi > 90°$), and its axes ratio is equal to $\tan(\Psi/2)$ (for $\Psi < 90°$) or $\cot(\Psi/2)$ (for $\Psi > 90°$).

Figure 2 illustrates how depolarization ratios depend on the reflectivity-weighted mean particle aspect ratio projection on the polarization plane, b, for the indicated transmitted polarizations and for planar- and columnar-type scatterers. It was assumed that the isolation between polarization channels is 35 dB. The presented results correspond to scatterers with their major dimensions randomly oriented in the horizontal plane and viewed at low elevations for planar particles (Figs. 2a and 2b) and viewed vertically for columnar particles (Figs. 2c and 2d). To illustrate the effect of particle bulk density ρ, the data are given for $\rho = 0.916$ g cm^{-3} (solid ice) and $\rho = 0.6$ g cm^{-3} (spongy ice).

The data of Fig. 2 show that there is an obvious trade-off between the desired increase in the weak channel intensity and dynamic range of DR. The amount of the signal increase in the weak channel when using these elliptical polarizations versus circular polarization can be easily estimated from Fig. 2 for particles of different shapes because, as stated above, the signal level in the strong channel changes very little.

Note from Fig. 2 that the polarization used in the ETL K_a-band radar in 1992–94 field experiments provides a nearly linear DR–b dependence (see curves 5) for planar crystals. The dynamic range of this depen-

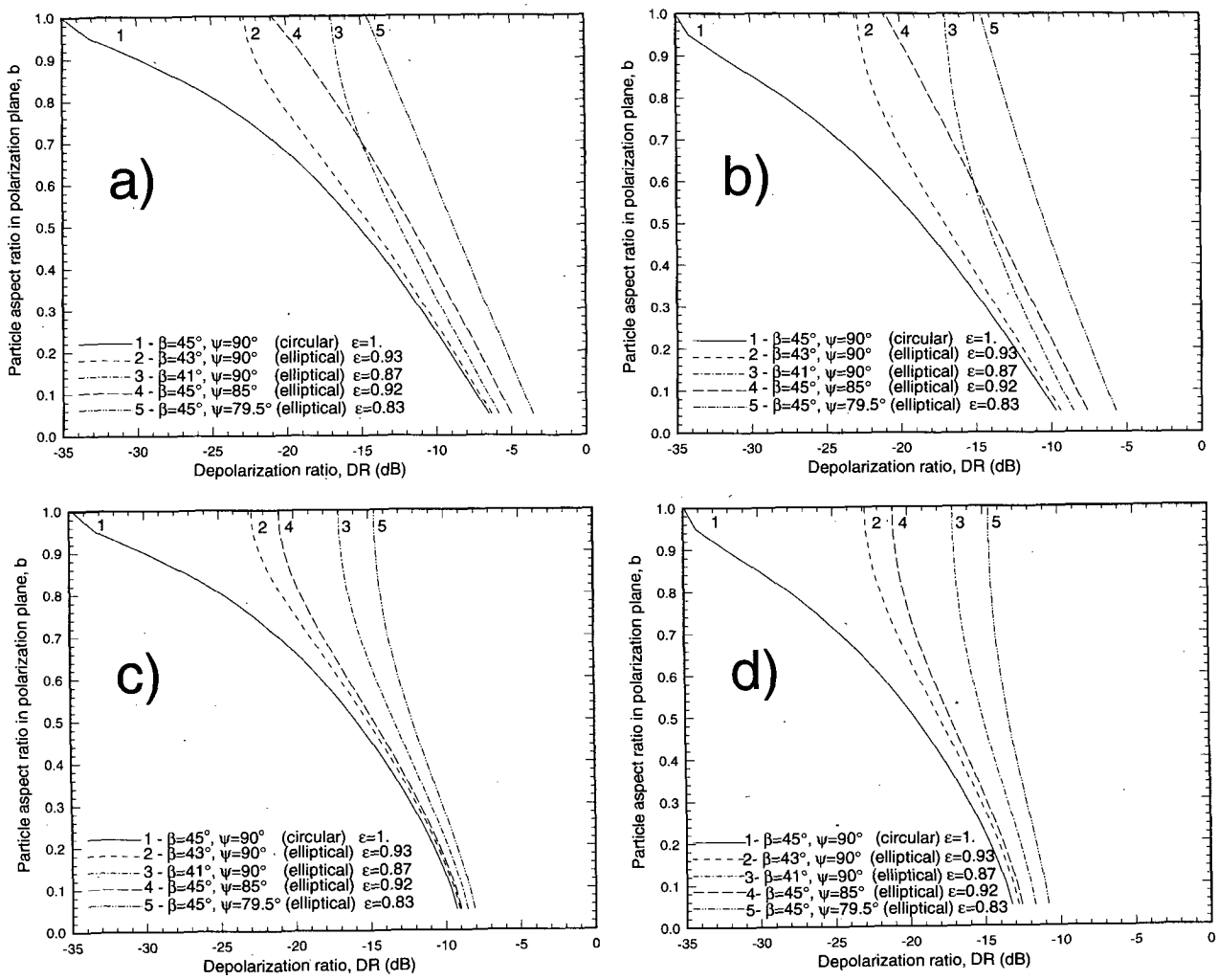

FIG. 2. Depolarization ratio DR on the circular and different elliptical polarizations as a function of the reflectivity-weighted particle mean aspect ratio in the polarization plane b for oblate [(a) and (b)] and prolate [(c) and (d)] particles and two bulk densities $\rho = 0.916$ g cm^{-3} [(a) and (c)], and $\rho = 0.6$ g cm^{-3} [(b) and (d)].

TABLE 1. Coefficients in the bulk density-size and thickness-major dimension relationships Eqs. (6)–(9) for different ice crystals. [Data from Pruppacher and Klett (1978), Heymsfield (1972), Auer and Veal (1970), Jayaweera and Cottis (1969), and Jayaweera and Ohtake (1974).] Dimensions are in centimeters and densities are in grams per cubic centimeter.

Crystal class	a_2	f	a_1	c
Dendrites, P1e	0.009	0.377	0.25	−0.377
Solid thick plates, C1g	0.138	0.778	0.916	0.0
Hexagonal plates, P1a	0.014	0.474	0.916	0.0
Solid columns, C1e ($L/d \leq 2$)	0.578	0.958	0.916	0.0
Solid columns, C1e ($L/d > 2$)	0.260	0.927	0.916	0.0
Hollow columns, C1f ($L/d \leq 2$)	0.422	0.892	0.53	−0.092 cold region
			0.82	−0.014 warm region
Hollow columns, C1f ($L/d > 2$)	0.263	0.930	0.53	−0.092 cold region
			0.82	−0.014 warm region
Long solid columns, N1e	0.035	0.437	0.916	0.0
Solid bullets, C1c ($L \leq 0.03$ cm)	0.153	0.786	0.916	0.0
Hollow bullets, C1d ($L > 0.03$ cm)	0.063	0.532	0.77	−0.0038
Elementary needles, N1a ($L < 0.05$ cm)	0.030	0.611	0.916	0.0

dence is less for columnar crystals and it also decreases with decreasing particle bulk density ρ.

3. Elevation angle dependence of elliptical depolarization ratios

It was shown theoretically (Matrosov 1991a) that planar crystals can be distinguished from columnar crystals by the elevation-angle dependence of CDR or LDR. Both LDR and CDR diminish as the elevation angle increases for plates, which is the opposite of the variation expected for columns. Here we extend the analysis to elliptical polarizations.

Modeling the elevation angle dependencies of ice particle depolarization ratios was performed for the elliptical polarization achievable with the PRP orientation of $\beta = 45°$ and a PRP phase shift of $\Psi = 79.5°$, the best estimate of its actual value. These were the parameters appropriate for data obtained with the ETL K_a-band radar during experiments in 1992–94. As discussed above, the PRP orientation $\beta = 45°$, used in a great majority of our measurements, would have produced circular polarization only if the PRP phase shift had been exactly 90°.

Planar and columnar crystals were simulated by oblate and prolate spheroids, which, as mentioned above, is justified because details of the particle shape are not as important to backscattering properties as is the overall particle shape. Shape is specified simply by the ratio of the particle minor to major axis. For this simulation, therefore, columnar crystals are represented by prolate spheroids and planar crystals by oblate spheroids. The Rayleigh theory (see, for example, Bohren and Huffman 1983) was used for these calculations because it gives acceptable results (with an accuracy better than about 30%) for solid ice particles smaller than about 1–1.5 mm at radar frequencies up to 35 GHz (Matrosov 1993; Schneider and Stephens 1994). Aggregate particles greater than 1.5 mm are usually optically "soft," and the simple Rayleigh–Gans theory is applicable in this case (Matrosov 1992).

It was assumed in the calculations that particles were oriented with their major dimensions primarily in the horizontal plane. Such orientation is determined by aerodynamic forcing (Mazin and Khrgian 1989; Sassen 1980) in the absence of strong turbulence and electric fields. The horizontal orientation was assumed to be random and different standard deviations σ_θ were considered for departures of the major particle dimensions from the horizontal.

a. Plates and dendrites

Plates and dendrites are among the most common crystal types observed in ice clouds and precipitation. Although shape is obviously a very important factor in determining the depolarization ratio, bulk density of the particle also has a major influence. For a given shape, the depolarization ratio increases with bulk density.

Hexagonal plates P1a and solid thick plates C1g usually, have the solid ice bulk density $\rho = 0.916$ g cm^{-3}. Hereafter, all particle-type indices are given according to the Magono and Lee classification. The bulk density ρ of dendrites P1e diminishes with crystal diameters D due to growth in a skeletal fashion (Pruppacher and Klett 1978):

$$\rho = a_1 D^c. \tag{5}$$

Similarly, aspect ratios of ice crystals are size dependent (Heymsfield 1972; Auer and Veal 1970; Jayaweera and Cottis 1969; Jayaweera and Ohtake 1974) and relations between crystal thicknesses h and their diameters can also be given by a power law such as

$$h = a_2 D^f. \tag{6}$$

Coefficients a_1, a_2, c, f in (5) and (6) are listed in Table 1.

Calculations of depolarization ratios require knowledge of the complex refractive index of ice particles. These are often considered to be an ice–air mixture (Rozenberg 1972) for particles with bulk density ρ, less than that for solid ice. Thus, the complex refractive index m of the air–ice mixture can be calculated using Wiener's equation, which, for this case, reduces to

$$\frac{m^2 - 1}{m^2 + 2} \approx \left(\frac{\rho}{\rho_i}\right) \frac{m_i^2 - 1}{m_i^2 + 2}, \tag{7}$$

where ρ_i and m_i are the density and complex refractive index of solid ice.

It is assumed that particle size distributions are described by the gamma function of the first order. This assumption is based on findings (Kosarev and Mazin 1991) that indicate that gamma functions of orders 0, 1, and 2 usually satisfactorily describe the observed distributions of ice particles. Having the order of the gamma functions specified reduces the number of variables to 3: particle concentration and median volume size, and deviation from the horizontal orientation. Total particle concentrations influence only the radar reflectivity and not depolarization ratios except in providing enough return echo to be measurable.

Figure 3 shows how DR values depend on the radar elevation angle χ for planar crystals with preferred horizontal orientation ($\sigma_\theta = 3°$). Results shown for hexagonal and thick plates are calculated for median volume diameters D_0 of 100 and 500 μm. Dendrites are usually larger so that, in this case, $D_0 = 200$ μm and $D_0 = 1$ mm were used. Depolarization ratios for solid ice plates (P1a, C1g) depend primarily on the reflectivity-weighted mean particle aspect ratio in the incident wave polarization plane. For dendrites (P1e), changes of crystal bulk density with particle size also influence depolarization.

It can be seen from Fig. 3 that there is a significant elevation angle dependence of depolarization ratios for planar crystals. However, the dynamic range of this dependence for the considered elliptical polarization ($\Psi = 79.5°$, and $\beta = 45°$) is less than for the circular polarization as discussed in Matrosov (1991a). The DR values at low elevation angles vary from about -3.8 to about -7.6 dB depending on the crystal characteristic size, density, and aspect ratio. Depolarization ratios decrease as the elevation angle increases and reach minimum values of about -14.8 dB, which is similar to DR for spherical particles observed with this elliptical polarization.

To evaluate more random particle orientations, calculations were also performed (not shown here) for $\sigma_\theta = 30°$. The general behavior of DR elevation angles dependencies remains close to ones shown in Fig. 3. The most important difference is in some decrease of the dynamic range of DR changes. For thick plates with $D_0 = 100$ μm, DR varies about 5 dB when χ increases from 0° to 90° for $\sigma_\theta = 30°$ compared to about 7 dB for $\sigma_\theta = 3°$. The elevation angle dependencies of DR still remain very pronounced.

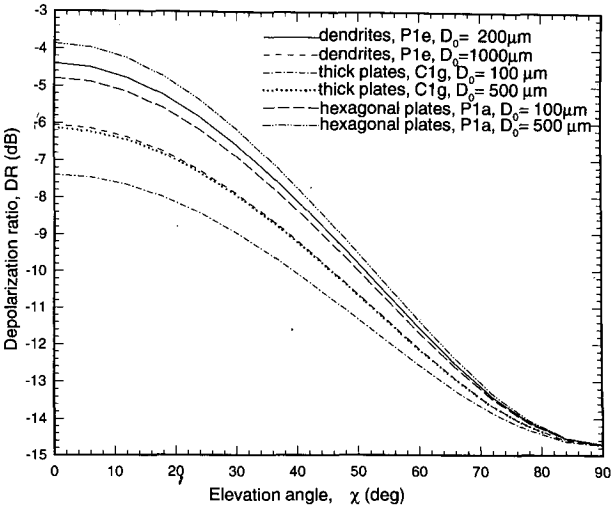

FIG. 3. Depolarization ratios of plate type ice crystals (P1e, C1g, P1a) as a function of radar elevation angle for elliptical polarization with $\beta = 45°$ and $\Psi = 79.5°$ and for different characteristic particle sizes.

The reflectivity-weighted mean particle aspect ratio in the polarization plane b for planar crystals can be estimated from data in Fig. 2. For a constant particle bulk density, the same mean aspect ratio can be produced by different combinations of χ, σ_θ, and the particle aspect ratio along the principal axes. Calculations with $3° < \sigma_\theta < 30°$, $0° < \chi < 90°$ and the elliptical polarization with $\Psi = 79.5°$ and $\beta = 45°$ show that these different combinations can result in an about 1–1.5 dB uncertainty in DR values for a fixed value of b.

b. Columns, needles, and bullets

The thicknesses of columnar crystals d and density ρ also depends on the crystal major dimension (i.e., crystal length L) and can be expressed as power laws similar to those for planar crystals as follows:

$$d = a_2 L^f, \tag{8}$$

$$\rho = a_1 L^c, \tag{9}$$

where values of coefficients a_1, a_2, c, and f compiled from Pruppacher and Klett (1978), Heymsfield (1972), Auer and Veal (1970), Jayaweera and Cottis (1969) and Jayaweera and Ohtake (1974) are also given in Table 1. Densities of solid crystals were assumed to be that of solid ice.

Calculations of elliptical depolarization ratios were performed for the most common columnar crystal classes found in ice clouds and precipitation. These classes include solid columns (C1e), hollow columns (C1f), elementary needles (N1a), long solid columns (N1e), solid bullets (C1c), and hollow bullets (C1d).

Figure 4 shows elevation-angle dependencies of depolarization ratios for solid and hollow columns ($\sigma_\theta = 3°$). Data for solid columns are shown for relatively small ($L_0 = 100$ μm) and large ($L_0 = 1$ mm) crystals and for elongated ($L/d > 2$) and blocky columns for which $L/d \leq 2$. Data for blocky hollow crystals are presented for densities typically found at cold temperatures ($T < -20°C$), and elongated hollow columns for warm temperatures. Hollow column sizes in cold regions are usually less than those in warm regions (Heymsfield 1972). Depolarization ratios of blocky hollow columns in warm regions and elongated hollow columns for cold regions (data are not shown) are within the limits of DR values shown in Fig. 4.

Figure 5 depicts DR–χ dependencies for needles, long solid columns, and solid and hollow bullets ($\sigma_\theta = 3°$). The solid-bullet DR data are shown for small particles and the hollow bullet data for large particles because of the higher likelihood of the presence of air within the larger bullets. Data shown in Figs. 4 and 5 illustrate that elongated crystals have considerably higher DR values than blocky crystals. Calculations for needles with $L_0 = 1$ mm were made for $\rho = 0.5$ g cm^{-3} rather than for solid ice density because of the likelihood of small amounts of air in crystal capillary spaces for large needles and sheath (N1c) (Pruppacher and Klett 1978).

The most distinguishing characteristic in elevation-angle dependencies of DR for columnar crystals is the trend of these dependencies. For the elliptical polarization transmitted by the ETL K_a-band radar ($\beta = 45°$, $\Psi = 79.5°$), there is a very small DR decrease with elevation. This is in contrast for CDR values that usually increase when the elevation angle χ increases (Matrosov 1991a). However, the decrease in DR values usually does not exceed 1.5 dB as χ increases from 0° to 90°.

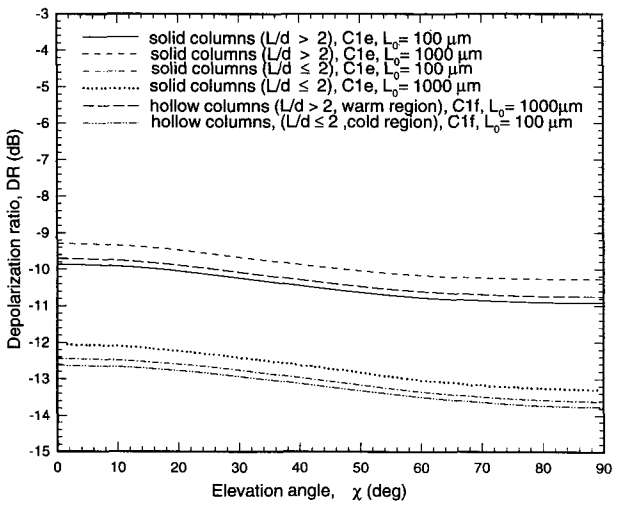

FIG. 4. Same as Fig. 3 but for solid (C1e) and hollow (C1f) columns.

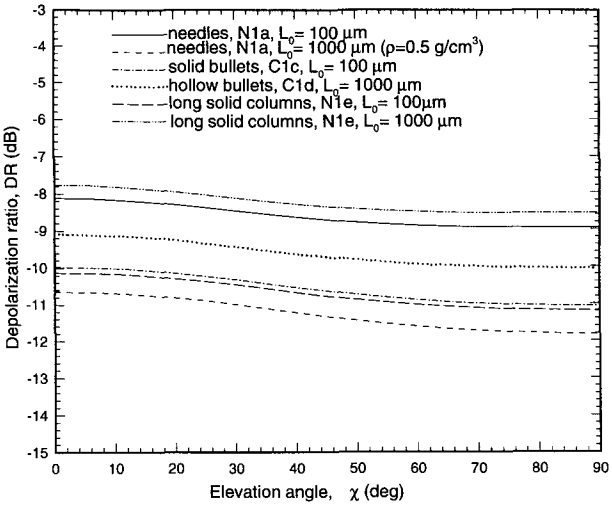

FIG. 5. Same as Fig. 3 but for needles (N1a), bullets (C1c, C1d), and long columns (N1e).

Such an elevation-angle trend results from the transmitted elliptical polarization being close to the "null" polarization (Kennaugh 1981; Boerner et al. 1981) for some prolates oriented with their major dimensions perpendicular to the electrical vector of the horizontal polarization ($\beta = 0°$). The very weak elevation-angle trend of DR for columnar crystals is rather convenient for estimations of mean particle aspect ratio. These estimations can be, however, rather crude because of relatively small dynamic range of DR due to particle aspect ratio changes. The elevation angle dependencies of DR can be more pronounced if the particle orientation in the horizontal plane is significantly not random.

As in the case of planar crystals, calculations were also performed for greater columnar particle deviations from the horizontal. Assuming $\sigma_\theta = 30°$ rather than $\sigma_\theta = 3°$ results in only about 0.5–1-dB reduction of DR compared to values shown in Figs. 4 and 5.

Planar and columnar particles considered above do not comprise all the possible natural crystal types. Figures 3, 4, and 5, however, give a good idea of variability in DR values and their elevation angle dependencies due to commonly found crystals.

c. *Aggregates*

Aggregates are conglomerates of ice crystals that usually have complex irregular shapes. The bulk density of aggregate particles is less than that of single shape crystals. In terms of aggregate particle major dimensions S (mm), this density can be approximated as (Illingworth 1994)

$$\rho \text{ (g cm}^{-3}) = 0.07 S^{-1.1}. \quad (10)$$

For $S < 97$ μm, it is assumed that $\rho = 0.916$ g cm^{-3}.

Because of the extreme complexity of aggregate shapes, they were also modeled as spheroids. To account for some natural shape diversity, aggregates were modeled by both oblate and prolate spheroids.

Figure 6 shows elevation-angle dependence of aggregate depolarization ratios. Sizes of aggregate particles can exceed those of pristine crystals. To account for this, modeling was performed for median volume particle sizes of 500 and 1500 μm. Larger aggregates would produce very low depolarization due to their low bulk densities. The aspect ratios used here (0.3 and 0.8) cover a fairly wide range of shapes. Note that to show details of the dependence, the DR scale in Fig. 6 was changed by a factor of 2 from that used in Figs. 3, 4, and 5.

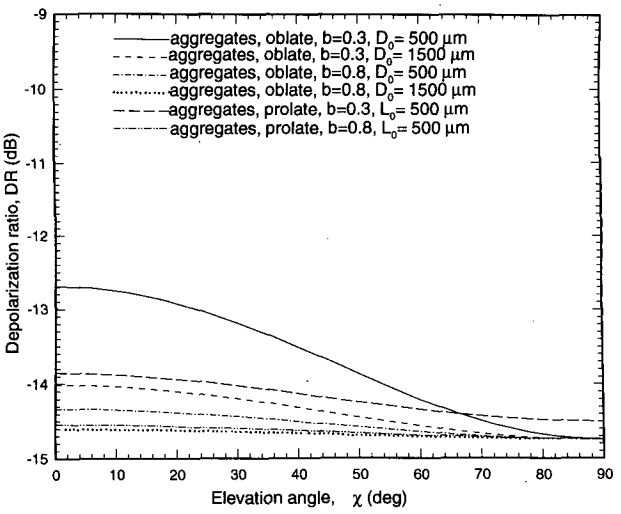

FIG. 6. Same as Fig. 3 but for aggregates.

d. Particle identification with elliptical polarization

The theoretical considerations discussed in this section were focused on the elliptical polarization that is currently transmitted by the ETL K_a-band radar. These considerations suggest that there is a good possibility for identification of particle types in ice clouds from dual-polarization measurements. Figure 3 shows that planar crystals have the elevation angle dependence of DR, which is very distinct from that of elongated columnar crystals and aggregates. Over the full 90° elevation-angle (χ) change, DR is seen to change by more than 7 dB (for $\sigma_\theta = 3°$) and 5 dB (for $\sigma_\theta = 30°$). Note also that the greatest absolute value of the derivative, $d\mathrm{DR}/d\chi$, can be observed when χ is from 40° to 60°.

Figures 4 and 5 show that the total variation of DR for columnar crystals does not generally exceed 1.5 dB. This is very distinct from planar crystals. The absolute value of the derivative $d\mathrm{DR}/d\chi$ is very small for columnar crystals for all values of χ. For elongated columnar crystals with $L/d > 2$, DR values are usually greater than -12 dB. Blocky crystals ($L/d \leq 2$) show generally low DR values; however, they are usually not found with values less than -14 dB.

The variation of depolarization ratios with elevation angle changes usually does not exceed about 2.5 dB for aggregates (see Fig. 6). At zenith, DR values are usually the lowest. For low density aggregates, depolarization ratios change little with the radar elevation angle χ. They are rather close to values expected from small water drops for the elliptical polarization transmitted by the ETL K_a-band radar.

Summarizing what was expressed above, one can conclude the following. 1) The dynamic range of DR changes, the derivative $d\mathrm{DR}/d\chi$ for $40° \leq \chi \leq 60°$, and the DR values near zenith direction ($\chi \approx 90°$) should be useful in distinguishing between planar crystals, columnar crystals, and aggregate ice particles. 2) Identifications based on the derivative $d\mathrm{DR}/d\chi$ should be most helpful when the entire dynamic range of DR changes is impossible to measure because of the absence of echoes at low or high elevations. 3) Reflectivity-weighted particle mean aspect ratios in the radar polarization plane can be estimated from DR–b dependencies for different bulk densities.

The DR-based differentiation between blocky ($L/d < 2$) columnar crystals and aggregates is, probably, the most difficult because both these hydrometeor types produce low depolarization. Generally, it can be expected that aggregates would produce less depolarization than columnar crystals due to their lower bulk density. However, an ambiguity between blocky columnar crystals and aggregates based solely on depolarization may still exist. To help resolve this ambiguity some additional information is needed. For example, the fact that blocky solid columns usually grow under conditions of very low water vapor supersaturation with respect to ice at the near equilibrium region can help with such differentiation.

Estimations of particle mean aspect ratios in the incident wave polarization plane (b) are potentially more accurate for planar crystals than for columnar crystals because of a greater dynamic range of DR changes due to changes in aspect ratios (see Figs. 2a and 2b vs Figs. 2c and 2d). For planar crystals randomly oriented in the horizontal plane with different deviations σ_θ, measurements of DR at different elevation angles χ provide estimates of b that change with χ due to changes in the relative geometry of the incident radar beam and particle orientation. For columnar crystals, DR changes very little with χ due to reasons discussed above. In this case estimates of b, obtained from data in Fig. 2c or 2d, will correspond to a mean horizontal projection of particle aspect ratios.

It is likely, however, that uncertainties in particle bulk densities and deviations from the preferred horizontal orientation along with measurements errors would allow only crude estimations of scatterer aspect ratios in the polarization plane. Particle shapes might be sorted into three or four categories.

4. Particle identification from observations of depolarization

An upslope snowstorm occurred in northeastern Colorado on 11–12 March 1993 during the WISPIT experiment (Reinking et al. 1993) providing a good opportunity to test some of the particle identification approaches discussed above. During the experiment, the NOAA K_a-band radar was located near Platteville, Colorado. The PRP configuration for these measurements was $\Psi \approx 79.5°$ and $\beta = 45°$, as described earlier.

Figure 7 shows observed fields of DR for three range–height indicator (RHI) scans in a vertical plane oriented at 14.5° azimuth. Around 2057 UTC 11 March (Fig. 7a) pristine dendritic crystals of about 1-mm diameter were observed at the radar. A sample of the observed crystals is also shown in the figure.

About 2h later (2253 UTC) precipitation observed near the radar consisted mostly of aggregates of dendrites and also some smaller irregular aggregate particles. The corresponding RHI scan is shown in Fig. 7c, along with crystal samples collected at the radar site.

Still later (0001 UTC 12 March), particles intermediate to the two above cases were observed and are shown in Fig. 7b. During this time period, mixed irregular aggregates and rimed single dendrites were observed.

a. The dendritic crystal case

Figure 8 shows experimental and calculated values of DR for the dendritic case shown in Fig. 7a at a range of 400 m. The data are nearly symmetrical relative to the zenith direction, suggesting a uniform cloud of crystals. This approximate symmetry was observed at ranges up to about 2 km (see Fig. 7a). As before, calculations were performed, with the assumption that the preferred orientation of ice crystals was randomly horizontal with a standard deviation $\sigma_\theta = 3°$ and the PRP phase shift was 79.5°. The bulk density and principal axes ratios for dendrites were modeled using data from Table 1. The dynamic range of observed DR values was about 8.5 dB ± 1 dB.

A general agreement between theoretical and experimental results is remarkably good given the uncertainties for the particle dimensions and densities for dendritic crystals [(5)–(6)]. Experimental data show somewhat lower values of DR near $\chi \approx 90°$ compared to calculated values. Theoretical data for this elevation are close to the spherical particle value of about −14.8 dB for the ETL K_a-band radar with its present PRP. One possible reason for this small discrepancy could be an uncertainty in the estimation of the PRP phase shift Ψ. An increase in Ψ would shift calculated depolarization ratios near $\chi = 90°$ to smaller values.

b. The aggregate case

Unlike the dendritic case, the aggregate case was not fully symmetrical relative to the zenith direction. As can be seen from Fig. 7c, somewhat larger DR values were measured at low elevations toward 14.5° azimuth than were observed in the opposite direction. Higher DR values were also observed in upper parts of the cloud. The areas of higher depolarization most probably contained pristine ice crystals at high concentrations.

To analyze this aggregate case, which appears to be somewhat inhomogeneous, and to reduce the influence of pristine crystals, the elevation angle dependence is shown in Fig. 9 for a constant altitude of 500 m rather than for a constant range. Optically "soft" aggregated particles cause much smaller propagation effects than single pristine crystals, and the use of constant altitude elevation angle dependencies (which results in larger propagation paths at low elevations) is justified.

The aggregated particles during this case varied from conglomerates of several dendrite crystals to much smaller, and therefore denser, irregularly shaped particles (see Fig. 7c). This probably resulted in smaller median sizes compared with the pure dendritic case. Model calculations were performed and shown in Fig. 9 for median volume particle sizes of 500 μm. To account for diversity of possible aggregate shapes and because of difficulties of measuring and modeling irregular shapes, calculations were made for both oblates and prolates.

It can be seen from Fig. 9 that the measurement data for $\chi > 100°$ should agree with theoretical calculations for prolate aggregates. The data for $\chi < 80°$ are in a better agreement with calculations for oblates, which also can be explained by a small contribution of dendrites probably existing there in small numbers. In general, the measured values of depolarization are very low and within those expected from aggregates (see Fig. 6).

5. Conclusions

It has been suggested that radar depolarization ratios can be used to determine the type and shape of ice hydrometeors. Circular depolarization ratios depend on the reflectivity-weighted particle mean aspect ratio in the incident wave polarization plane while linear depolarization ratios depend on this ratio and particle orientations in the incident wave polarization plane. For low reflectivity scatterers, that is, when echoes in the weak polarization channel are below the detectability threshold, the use of elliptical polarization with ellipticity close to 1 (such as transmitted by the ETL K_a-band radar) provides possibility of depolarization measurements unavailable with traditional circular and linear polarizations. The signal in the weak channel is enhanced, while the strong echo does not change significantly when such elliptical rather than circular polarization is used. This comes, however, with a disadvantage of decreased variations of depolarization ratios with respect to particle shapes and more ambiguous data interpretation.

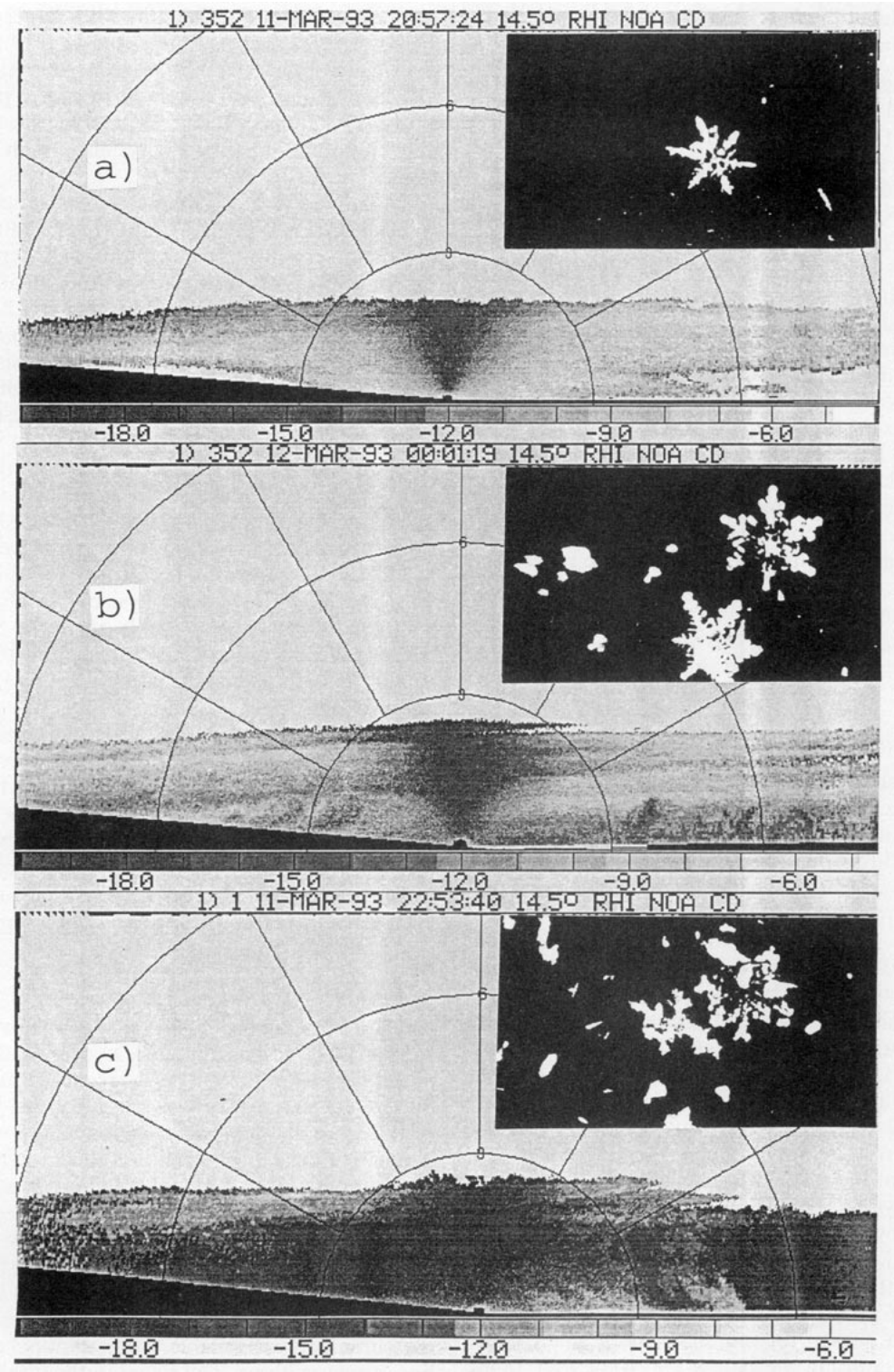

FIG. 7. Elevation-angle dependencies of depolarization ratios measured at the 14.5 azimuth during the WISPIT snow storm event on 11–12 March 1993: (a) case of pristine dendrite crystals, (b) case of rimed dendrites mixed with small aggregates, and (c) case of dendrite aggregates and smaller irregular shape aggregates. Photographs of sampled particles are shown for each case. Range rings are 3 km apart.

Calibrations of the NOAA ETL K_a-band radar during the 1992–94 field programs indicated that an elliptical polarization with ellipticity of about 0.83 was used rather than the true circular polarization. Theoretical studies of depolarization expected from different ice hydrometeors were performed for this elliptical polarization and different deviations of crystals from the preferred horizontal orientation.

Results of the model calculations showed that randomly oriented in the horizontal plane, planar crystals, columnar crystals, and aggregates have distinctly different variations of DR with elevation angle. The range of DR values for planar crystals usually exceeds about 5 dB when elevation is varied from 0° to 90°. For columnar crystals and aggregates this range is much less. Elongated single-shape columnar crystals theoretically show depolarization ratios from about −8 to −11 dB. Blocky columnar crystals and aggregates produce lower depolarization, generally less than −12 dB. This suggests a possibility of distinguishing between planar crystals, columnar crystals, and aggregates and blocky crystals. For more reliable differentiations between blocky columnar crystals and aggregates, information about water vapor supersaturation with respect to ice might be useful.

For a particular particle type, the reflectivity-weighted mean particle aspect ratio in the incident wave polarization plane can be estimated from depolarization ratios. This ratio, probably, can be estimated in three or four categories because of uncertainties in particle density and orientation.

The possibility of ice hydrometeor identification was illustrated using data obtained during the WISPIT experiment conducted in northeastern Colorado in 1993. Observed depolarization ratio dependencies on radar elevation angle for dendrites and aggregates showed generally good agreement with calculations and also demonstrated a clear distinction from theoretical values for elongated columnar crystals. The approaches described here are likely to have greater success in situations characterized by horizontal homogeneity in the absence of strong electrical fields and turbulence and also for cases where mostly single crystal types, rather than mixtures, are present in the radar sample volume.

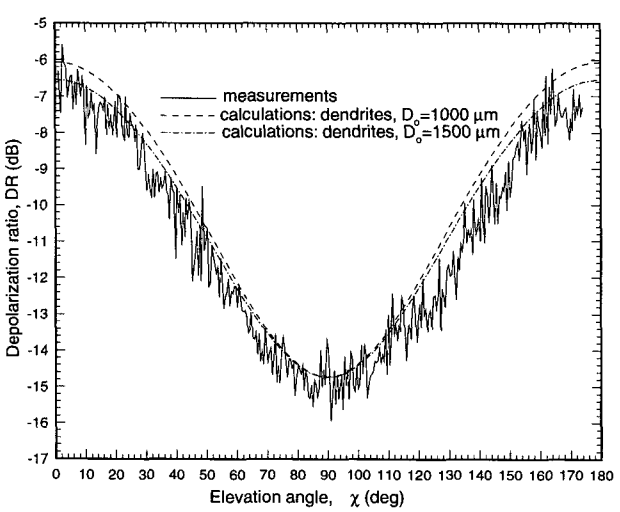

FIG. 8. Experimental elevation-angle dependence of dendrite crystal depolarization ratios at 2057:24 UTC. Angles $\chi < 90°$ correspond to the azimuth direction 14.5°. Also shown are calculated data.

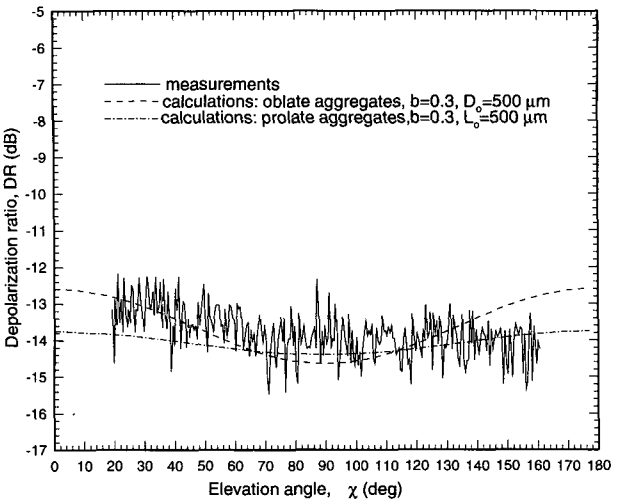

FIG. 9. Same as Fig. 8 but for the aggregate case at 2053:40 UTC.

Acknowledgments. This research was funded in part through a grant from the Environmental Science Division of the U.S. Department of Energy and an Interagency Agreement in response to requirements and funding by the Federal Aviation Administration's Aviation Weather Development Program (FAA ARD-80) that was administered by the National Science Foundation. Brooks E. Martner and Brad W. Orr of NOAA/ETL helped to acquire the radar data.

REFERENCES

Auer, A. H., and D. L. Veal, 1970: The dimension of ice crystals in natural clouds. *J. Atmos. Sci.*, **27**, 919–926.

Boerner, W.-M., M. B. El-Arini, C. Y. Chan, and P. M. Mastoris, 1981: Polarization dependence in electromagnetic inverse problems. *IEEE Trans. Antennas Propag.*, **AP-29**, 262–271.

Bohren, C. F., and D. R. Huffman, 1983: *Absorption and Scattering of Light by Small Particles.* John Wiley and Sons, 530 pp.

Chylek, P., and G. Videen, 1994: Longwave radiative properties of polydispersed hexagonal ice crystals. *J. Atmos. Sci.*, **51**, 175–190.

Doviak, R. J., and D. S. Zrnic, 1993: *Doppler Radar and Weather Observations.* Academic Press, 562 pp.

Dungey, C. E., and C. F. Bohren, 1993: Backscattering by nonspherical hydrometeors as calculated by the coupled-dipole method: An application in radar meteorology. *J. Atmos. Oceanic Technol.*, **10**, 526–532.

Fu, Q., and K. N. Liou, 1993: Parameterization of the radiative properties of cirrus clouds. *J. Atmos. Sci.*, **50**, 2008–2025.

Heymsfield, A. J., 1972: Ice crystal terminal velocities. *J. Atmos. Sci.*, **29**, 1348–1357.

Jayaweera, K. O. L. F., and R. E. Cottis, 1969: Fall velocities of plate-like and columnar ice crystals. *Quart. J. Roy. Meteor. Soc.*, **55,** 703–709.

——, and T. Ohtake, 1974: Properties of columnar ice crystals precipitating from layer clouds. *J. Atmos. Sci.*, **31,** 280–286.

Illingworth, A. J., 1994: Spaceborne cloud radar: Sampling and retrievals. *Workshop on Cloud Profiling Radar, Global Energy and Water Cycle Experiment,* World Climate Research Programme, International GEWEX Program Office (IGPO), Publication Series No. 10, B48–B53.

Kennaugh, E. M., 1981: Polarization dependence on RCS—A geometrical interpretation. *IEEE Trans. Antennas Propag.*, **AP-29,** 412–413.

Kosarev, A. L., and I. P. Mazin, 1991: An empirical model of the physical structure of upper layer clouds. *Atmos. Res.*, **26,** 207–216.

Kropfli, R. A., B. W. Bartram, and S. Y. Matrosov, 1990: The upgraded WPL dual-polarization 8-mm wavelength Doppler radar for microphysical and climate research. *Proc. Conf. on Cloud Physics,* San Francisco, CA, Amer. Meteor. Soc., 341–345.

——, and R. D. Kelly, 1995: Meteorological research applications of mm-wavelength radar. *Meteorology and Atmospheric Physics,* in press.

Liou, K. N., and Y. Takano, 1994: Light scattering by nonspherical particles: Remote sensing and climatic implications. *Atmos. Res.*, **31,** 271–298.

Magono, S. C., and C. W. Lee, 1966: Meteorological classification of natural snow crystals. *J. Fac. Sci. Hokkaido Univ. Ser. VII,* **2,** 321–362.

Mason, B. J., 1994: The shape of snow crystals—Fitness for purpose? *Quart. J. Roy. Meteor. Soc.*, **120,** 849–860.

Matrosov, S. Y., 1991a: Theoretical study of radar polarization parameters obtained from cirrus clouds. *J. Atmos. Sci.*, **48,** 1062–1070.

——, 1991b: Prospects for the measurement of ice cloud particle shape and orientation with elliptically polarized radar signals. *Radio Sci.*, **26,** 847–856.

——, 1992: Radar reflectivity in snowfall. *IEEE Trans. Geosci. Remote Sens.*, **GE-30,** 454–461.

——, 1993: Possibilities of cirrus particle sizing from dual-frequency radar measurements. *J. Geophys. Res.*, **98**(D11), 20 675–20 683.

——, and R. A. Kropfli, 1993: Cirrus cloud studies with elliptically polarized K_a-band radar signals: A suggested approach. *J. Atmos. Oceanic Technol.*, **10,** 526–532.

Mazin, I. P., and A. K. Khrgian (editors), 1989: *Handbook of Clouds and Cloudy Atmosphere.* Hydrometeoizdat, 648 pp.

Pruppacher, H. R., and J. D. Klett, 1978: *Microphysics of Clouds and Precipitation.* D. Reidel, 714 pp.

Reinking, R. F., S. Y. Matrosov, B. E. Martner, R. A. Kropfli, and B. W. Bartram, 1995: Hydrometeor identification with millimeter-wave dual polarization radar. Preprints, *Conf. Cloud Phys.,* Dallas, TX, Amer. Meteor. Soc., 20–25.

——, B. W. Orr, B. B. Stankov, and C. A. Davis, 1993: NOAA K_a-band cloud sensing radar measurements during WISPIT. Preprints, *Fifth Int. Conf. on Aviation Weather Systems,* Vienna, VA, Amer. Meteor. Soc., 130–134.

Rozenberg, V. I., 1972: *Scattering and Extinction of Electromagnetic Radiation by Atmospheric Particles.* Hydrometeoizdat, 348 pp.

Sassen, K., 1980: Remote sensing of planar ice crystal fall attitudes. *J. Meteor. Soc. Japan,* **58**(5), 422–429.

Schneider, T. L., and G. L. Stephens, 1994: Backscattering by nonspherical ice particles at millimeter wavelengths: *Eighth Conf. on Atmospheric Radiation,* Amer. Meteor. Soc., Nashville, TN, 310–312.